Carbohydrate Polymers 92 (2013) 1124–1132

Contents lists available at SciVerse ScienceDirect

Carbohydrate Polymers

journal homepage: www.elsevier.com/locate/carbpol

Core–shell nanocarriers with ZnO quantum dots-conjugated Au nanoparticle for tumor-targeted drug delivery

Tong Chen [a], Tong Zhao [a], Dongfeng Wei [c], Yanxia Wei [c], Yuanyuan Li [a], Haixia Zhang [a,b,*]

[a] Key Laboratory of Nonferrous Metal Chemistry and Resources Utilization of Gansu Province, Lanzhou University, Lanzhou 730000, China
[b] Key Laboratory of Chemistry of Northwestern Plant Resources, Lanzhou Institute of Chemical Physics, Chinese Academy of Sciences, Lanzhou 730000, China
[c] School of Basic Medical Science, Lanzhou University, Lanzhou 730000, China

ARTICLE INFO

Article history:
Received 6 May 2012
Received in revised form 1 September 2012
Accepted 8 October 2012
Available online 17 October 2012

Keywords:
Nanocarriers
Drug delivery
ZnO quantum dots
Cytotoxicity

ABSTRACT

Core–shell structured multifunctional nanocarriers (NCs) of ZnO quantum dots-conjugated gold nanoparticles (Au NPs) as core and amphiphilic hyperbranched block copolymer as shell were synthesized for targeted anticancer drug delivery. The amphiphilic hyperbranched block copolymer contained poly(L-lactide) (PLA) inner arm and folate (FA)-conjugated a sulfated polysaccharide from *Gynostemma pentaphyllum* Makino (GPPS-FA) outer arm. The structure and properties of core–shell structured multifunctional nanocarriers were characterized and determined by UV–visible spectra, FT-IR spectra, X-ray diffraction (XRD), fluorescence spectroscopy and TEM analyses. The release results indicated that camptothecin (CPT) release from NCs at pH 7.4 was much greater than that at pH 5.3. The cytotoxicity studies showed that both the blank NCs and the CPT-loaded NCs provided high anticancer activity against Hela cells. Furthermore, nanocarriers gained specificity to target model cancer cells in this study due to the enhanced cell uptake mediated by FA moiety. The results indicated that the NCs not only had great potential as tumor-targeted drug delivery nanocarrier, but also had an assistant role in the treatment of cancer.

1. Introduction

The application of nanotechnology to biological science is widely expected to change the landscape of pharmaceutical and biotechnology industries for the foreseeable future (Wu, Shen, Banerjee, & Zhou, 2010; Yuan et al., 2011). Quantum dots (QDs) with narrow size distribution and high luminescent efficiency have attracted attention of researchers due to their wide applications in the areas of biological fluorescence labeling and medical research (Chan & Nie, 1998). Compared with the conventional dyes used as imaging probes, QDs have several advantages in optical and chemical properties, such as tunable emission from visible to infrared wavelengths by changing their size and composition, broader excitation spectra due to high absorption coefficients, high quantum yield of fluorescence, strong brightness, photostability, and high resistance to photobleaching. These unique properties of QDs have attracted tremendous interest in exploiting them in a variety of biological fields (Alivisatos, Gu, & Larabell, 2005; Medintz, Uyeda, Goldman, & Mattoussi, 2005; Michalet et al., 2005). However, the potential applications of QDs in biology and medicine are limited due to the toxic effects of semiconductor QDs, which has received enormous attention over the past few years (Bottrill & Mark, 2011; Yuan, Hein, & Misra, 2010). Comparing with the traditionally II–VI group QDs, such as CdSe and CdTe QDs, ZnO QDs are cheap and biocompatible to the biological systems (Xiong, Xu, Ren, & Xia, 2008), which inspires great interest in biological labeling and photocatalytic applications. ZnO QDs are noncytotoxic and its strong fluorescence is fit for bioimaging (Moussodia, Balan, Merlin, Mustin, & Schneider, 2010; Viswanatha, Chakraborty, Basu, & Sarma, 2006; Zeng et al., 2007).

Gold nanoparticles (Au NPs) have received considerable attention during the past decade due to their potential applications in catalysis, chemical sensing, electronics, optics and biology (Luo, Xu, Zhang, Liu, & Wu, 2005; Prabaharan, Grailer, Pilla, Steeber, & Gong, 2009a; Prabaharan, Grailer, Pilla, Steeber, & Gong, 2009b; Reum et al., 2010). Au NPs are also an ideal drug-delivery scaffold because they are known to be nontoxic and nonimmunogenic (Cheng et al., 2010; Duncan, Kim, & Vincent, 2010; Male, Lachance, Hrapovic, Sunahara, & Luong, 2008). Au NPs have recently emerged as an attractive candidate for delivering various therapeutic agents such as drugs, peptides, proteins, and nucleic acids into their targets (Ghosh, Han, De, Kim, & Rotello, 2008). For example, Brown et al. have tethered the active component of the anticancer drug

* Corresponding author at: Key Laboratory of Nonferrous Metal Chemistry and Resources Utilization of Gansu Province, Lanzhou University, Lanzhou 730000, China. Tel.: +86 931 8912510; fax: +86 931 8912582.
E-mail addresses: chentong2006@163.com (T. Chen), zhanghx@lzu.edu.cn (H. Zhang).

0144-8617/$ – see front matter © 2012 Elsevier Ltd. All rights reserved.
http://dx.doi.org/10.1016/j.carbpol.2012.10.022

oxaliplatin to Au NPs for improved drug delivery (Sarah, Brown Nativo, Smith, Stirling, & Edwards, 2010). Particularly, Au NPs can be used to destroy the tumor cells without damaging the surrounding tissue by photo-thermal therapy since they can efficiently convert the absorbed laser light energy into localized heat (Jain, Ih, & Ma, 2007). Finally, due to their intense light scattering power, Au NPs targeted to cancer tissue may improve surgeons' ability to identify metastatic lesions.

Polysaccharides from plants are not only safe, biocompatible, but also biodegradable, which own many kinds of biological activities. Furthermore, molecular modification of polysaccharide was considered as a way to enhance the biological activities of polysaccharide. Recently, polysaccharide obtained from *Gynostemma pentaphyllum* Makino (GPP) has attracted great attention owing to its antitumor activities, immunomodulatory effect and antioxidant properties (Birgitte, Per, & Zhao, 1995; Qian, Wang, & Tang, 1998; Rujjanawate, Kanjanapothi, & Amornlerdpison, 2004). In our previous work, GPP with molecular mass (M_w) as 9.3 kDa was obtained containing the composition of rhamnose and xylose, whose mol ratio was 1:12.25. The glucosidic bond configuration of the GPP was mainly α-configuration. We synthesized the sulfated derivatives of GPP (GPPS) by chlorosulfonic acid–pyridine method, and the product showed that the degree of substitution (DS) was 1.20, and M_w was 8.96 kDa. The GPPS had higher antitumor activities than the GPP obviously (Chen et al., 2011). Based on the above experimental results, GPPS could be used as a hydrophilic outer shell of drug carriers for better biocompatible and antitumor activities but low cytotoxicity to normal cells.

In recent decades, cancer continues to be on the rise with increasing age of the population. The medical science has improved obviously, but conventional chemotherapeutic agents exhibit poor specificity in reaching tumor tissue and are often restricted by dose-limiting toxicity (Gu et al., 2007). The current focus in the development of cancer therapies is on targeted drug delivery to provide therapeutic concentrations of anticancer agents at the site of action and to spare the normal tissues (Jain, 2005). Folate (FA) is an attractive target ligand due to its high binding affinity for the folate receptors, and is efficiently internalized into the cells through the receptor-mediated endocytosis even when conjugated with a wide variety of molecules (Leamon & Low, 1991; Prabaharan et al., 2009a, 2009b; Turek, Leamon, & Low, 1993; Zhu, Fang, & Kaskel, 2010).

To the best of our knowledge, there was still no reported study on drug carriers themselves with certain antitumor activities due to GPPS as a hydrophilic outer shell. In this study, we synthesized core–shell structured multifunctional nanocarriers (ZnO-Au-PLA-GPPS-FA) of ZnO quantum dots-conjugated Au NPs as core and FA-conjugated amphiphilic hyperbranched block copolymer as shell based on poly(L-lactide) (PLA) inner arm and FA-conjugated GPPS (GPPS-FA) outer arm for targeted anticancer drug delivery. ZnO QDs-conjugated Au NPs could be used for fluorescence labeling and destroying the tumor cells by photo-thermal therapy, respectively. Both the inner hydrophobic block (PLA) and the outer hydrophilic block (GPPS-FA) were biodegradable and biocompatible. FA-conjugated nanocarriers (NCs) could be directed to the cancer cells and subsequently internalized in the target cell *via* receptor-mediated endocytosis. Furthermore, NCs themselves had certain antitumor activities due to GPPS on their surface. The structure and properties of NCs were characterized and determined by UV spectra, FT-IR spectra, XRD, DLS, fluorescence spectroscopy and TEM analyses. The drug loading and *in vitro* release studies were performed using camptothecin (CPT) as a hydrophobic model anticancer drug. *In vitro* cytotoxicity of NCs were investigated by employing Hela cells through the 3-(4,5-dimethylthiazol-2-yl)-2,5-diphenyltetrazolium bromide (MTT) assay.

2. Experimental

2.1. Materials and reagents

The crude GPP from *G. pentaphyllum* Makino (collected from the mountain area in Weinan City, Shaanxi Province, China) was obtained from Shaanxi Lixin Biotechnology Co. (China) and purified further in our laboratory. M_w of purified GPP was 9.3 kDa and its composition contained rhamnose and xylose, whose mol ratio was 1:12.25. The sulfated derivatives of GPP (GPPS) showed that the DS was 1.20, and M_w was 8.96 kDa (Chen et al., 2011). The purification and FT-IR spectra (Fig. S1) of GPP were shown in supporting information.

Potassium hydroxide (KOH), triethylamine and FA were purchased from Tianjin Guangfu Chemical Research Institute (Tianjin, China). 1-(3-Dimethylaminopropyl)-3-ethylcarbodiimide hydrochloride (EDC·HCl), tetrachloroauric acid ($HAuCl_4$), N-hydroxy succinimide (NHS), 2-aminoethanethiol (AET), mercaptoacetic acid (MAA) and 4-dimethylamino pyridine (DMAP) were purchased from Aladdin Chemistry Co., Ltd. (Beijing, China). Tri-sodium citrate, sodium borohydride ($NaBH_4$) and succinic anhydride were obtained from Sinopharm Chemical Reagent Co., Ltd. (Beijing, China). PLA (M_w, 10 kDa and 15 kDa) was purchased from Brightchina Co., Ltd. CPT was supplied by Lanbei Plant & Chemical Co., Ltd. (Chengdu, China). N,N-Dimethylformamide (DMF), ethanol and dichloromethane (CH_2Cl_2) were analytical grade and obtained from Gansu Yinguang Chemical Industry Co. (China). MTT was from Sigma Co. (France).

2.2. Synthesis of amine functionalized ZnO QDs

ZnO QDs were first obtained by the method of literature (Patra et al., 2009). Thereafter, 500 mg of ZnO was dispersed in 50 mL of ethanol. 24 mg of AET was added into the above ZnO solution under stirring at room temperature. After 24 h, the resulting amine functionalized ZnO particles were obtained by centrifugation, washed with ethanol three times, and followed by drying in vacuum.

2.3. Synthesis of carboxyl functionalized Au NPs

Au NPs were synthesized by the $NaBH_4$ reduction method (Jana, Gearheart, & Murphy, 2001). Then 340 μL of MAA was added into 100 mL of aqueous solution containing Au NPs (20 mg) under vigorous stirring at room temperature. After 24 h, the resulting thiol stabilized Au NPs were followed by dialysis against deionized water for 48 h to obtain the carboxyl functionalized Au NPs.

2.4. Synthesis of ZnO QDs-conjugated Au NPs

Fifteen milligrams of the carboxyl functionalized Au NPs was suspended in 10 mL of anhydrous DMF, and the surface carboxyl groups were activated by adding 50 mg of NHS and 90 mg of EDC·HCl and stirred well at room temperature for 2 h. Then 2 g of the amine functionalized ZnO QDs in 20 mL of anhydrous DMF was added quickly. The mixture was stirred at room temperature for 24 h. Finally, ZnO QDs-conjugated Au NPs were collected by filtration, washed with ethanol three times, and followed by drying in vacuum.

2.5. Synthesis of ZnO-Au-PLA

ZnO QDs-conjugated Au NPs (1 g) was suspended in 20 mL of anhydrous CH_2Cl_2, and the surface carboxyl groups were activated by adding 40 mg of NHS and 80 mg of EDC·HCl and stirred at room temperature for 2 h. Then 3 g of PLA (M_w, 10 kDa and 15 kDa) in 50 mL of anhydrous CH_2Cl_2 was added, respectively. After 48 h, the

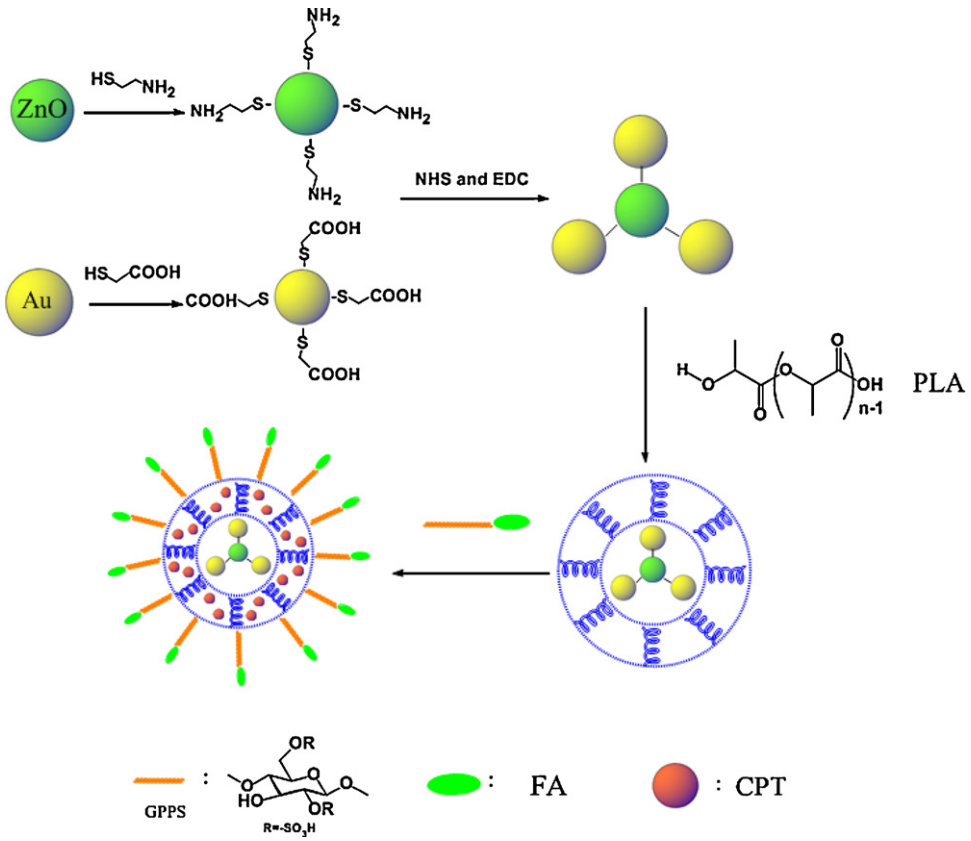

Fig. 1. Preparation procedures of the ZnO-Au-PLA-GPPS-FA NCs.

reaction mixture was poured into cold diethyl ether, and a precipitate was collected by filtration and washed with diethyl ether, followed by drying in vacuum. The products were denoted as ZnO-Au-PLA-1 and ZnO-Au-PLA-2.

2.6. Synthesis of FA-conjugated GPPS

FA (100 mg) was added into 20 mL of anhydrous DMF and stirred in the dark. Then, the FA solution was mixed with 50 mg of EDC·HCl and 30 mg of DMAP and stirred for 5 h. 1 g of GPPS was added to the mixture and the reaction was carried out in the dark for 24 h. The product, GPPS-FA was dialyzed against deionized water using a dialysis tubing (molecular weight cut-off of 3 kDa) for 48 h and freeze-dried.

2.7. Synthesis of ZnO-Au-PLA-GPPS-FA

ZnO-Au-PLA-GPPS-FA NCs was synthesized by reacting the carboxyl groups of ZnO-Au-PLA with the hydroxyl group of GPPS-FA in the presence of EDC·HCl and DMAP as the catalysts. ZnO-Au-PLA (200 mg) was suspended in 20 mL of anhydrous DMF, EDC·HCl (20 mg) and DMAP (10 mg) were added and stirred at room temperature for 5 h. Then, 600 mg of GPPS-FA in 30 mL of anhydrous DMF was added dropwise into the reaction mixture. The reaction was carried out at room temperature for 24 h under stirring. Finally, the product was then dialyzed against deionized water for 48 h (molecular weight cut-off of 12 kDa) and freeze-dried. The products were denoted as ZnO-Au-PLA-GPPS-FA-1 and ZnO-Au-PLA-GPPS-FA-2.

The routes for synthesis of core–shell structured multifunctional NCs (ZnO-Au-PLA-GPPS-FA) were showed in Fig. 1.

2.8. Characterization

Absorbance spectra and measurements were carried out using a Puxi UV-1810 visible spectrophotometer (Beijing, China). The IR spectra were recorded on a Nicolet 20 NEXUS 670 FT-IR spectrophotometer (Ramsey, MA, USA) using KBr pellets. The XRD patterns from 5° to 80° were recorded on a X'PertPro (RANalypical, Holland) using Cu Kα radiation. Fluorescence spectra of ZnO QDs and NCs were recorded on a RF-5301PC fluorescence spectrometer (Shimadzu, Japan) at room temperature. The sizes of ZnO QDs, Au NPs and NCs were determined by a BI-200SM DLS (Brookhaven, USA) with angle detection at 90°. The morphology of ZnO QDs, Au NPs and NCs were recorded by a Tecnai-G2-F30 TEM (FEI, USA).

2.9. Drug loading and release in vitro

CPT was loaded into the NCs as follows: 30 mg of CPT was dissolved in 30 mL of DMF, and the NCs (30 mg) were added under stirring at room temperature. After stirring 24 h, the suspension was centrifuged for 10 min at 10,000 rpm. To remove free CPT, the precipitate was further washed by three times using DMF. All the upper clear solutions were collected, and the concentration of free CPT was determined by UV–visible spectrometry at 366 nm. The amount of loaded CPT in the NCs was calculated from the decrease in CPT concentration. All the experiments were carried out in triplicate.

The *in vitro* release behavior was evaluated by the dialysis method. The release studies were performed at 37 °C in acetate buffer (pH 5.3) and phosphate buffer (PBS, pH 7.4) solutions. First, 30 mg of the CPT-loaded ZnO-Au-PLA-GPPS-FA NCs was dispersed in 5 mL of medium and placed in a dialysis bag with a molecular weight cut-off of 3 kDa. The dialysis bag was then immersed in 45 mL of the release medium and kept in a horizontal laboratory

shaker maintaining a constant temperature. Samples (1 mL) were periodically removed and the volume of each sample was replaced by the same volume of fresh medium. The amount of released CPT was analyzed with a spectrophotometer at 366 nm. The drug release studies were performed in triplicate for each of the samples.

2.10. In vitro cytotoxicity

The cytotoxicity of the free and the CPT-loaded NCs was assessed by using the MTT assay. For these studies, uterine cervix carcinoma cell line (Hela) and the human lung adenocarcinoma cell line (A549) were provided by the Biology Preservation Center in Shanghai Institute of Materia Medica and maintained with RPMI 1640 medium containing 10% fetal bovine serum (FBS), and 100 U/mL penicillin and 100 μg/mL streptomycin at 37 °C in a humidified atmosphere with 5% CO_2. The cells (1×10^4 cells/well) were seeded into 96-well plates and incubated for 24 h, respectively. Then the CPT-free NCs, the CPT-loaded NCs and the free CPT with different concentration were added. After incubation for 48 h at 37 °C, the culture medium was removed and 20 μL of MTT reagent (diluted in culture medium, 0.5 mg/mL) was added. Following incubation for 4 h, the MTT/medium was removed carefully and DMSO (150 μL) was added to each well for dissolving the formazan crystals. Absorbance of the colored solution was measured at 570 nm using a microplate reader (Bio-Rad, iMark™). All experiments were performed in triplicate.

3. Results and discussion

3.1. Synthesis of ZnO-Au-PLA-GPPS-FA

The reaction scheme of ZnO-Au-PLA-GPPS-FA NCs was shown in Fig. 1. First, ZnO QDs were prepared by a sol–gel process, and were functionalized with the amine groups by reacting AET on the monolayer of ZnO QDs through thiol linkers. Au NPs were prepared and functionalized with the carboxyl groups by reacting MAA through thiol linkers. To obtain ZnO QDs-conjugated Au NPs, the amine functionalized ZnO QDs were coupled with the carboxylic functionalized Au NPs by the amide linkage. The ZnO QDs-conjugated Au NPs as core was designed to emit fluorescent light for optical sensing and cellular imaging, as well as absorbed and converted laser light energy to heat for photo-thermal treatment.

In the second step, the NCs shell was synthesized by first coating a hydrophobic PLA layer onto NCs core and then using this hydrophobic layer as a seed for the subsequent formation of the hydrophilic GPPS-FA layer. ZnO-Au-PLA was synthesized by reacting the surface carboxyl groups of ZnO QDs-conjugated Au NPs with some of the terminal hydroxyl group of PLA by ester forming reaction. The PLA could provide hydrophobic network to load hydrophobic drug by hydrophobic–hydrophobic interactions. Then ZnO-Au-PLA-GPPS-FA NCs was obtained by reacting the terminal carboxyl group of ZnO-Au-PLA with some of the hydroxyl groups of GPPS-FA by ester forming reaction.

3.2. Structural characterization of ZnO-Au-PLA-GPPS-FA

The ZnO QDs and Au NPs were confirmed by UV–visible spectroscopy analysis, as shown in Fig. 2(I). The UV–visible spectra of ZnO QDs showed clear shifted band edge absorption at 340 nm. An empirical formula based on UV–visible absorption spectra had been given by Meulenkamp to calculate the size of ZnO QDs, which was applicable in the size range from 2.5 to 4.5 nm (Meulenkamp, 1998). The UV–visible spectra of Au NPs showed characteristic surface plasmon resonance (SPR) bands at 520 nm. The result indicated the formation and existence of Au NPs (Bahadur, Aryal, Bhattarai, & Kim, 2006; Wyrna & Beyer, 2002).

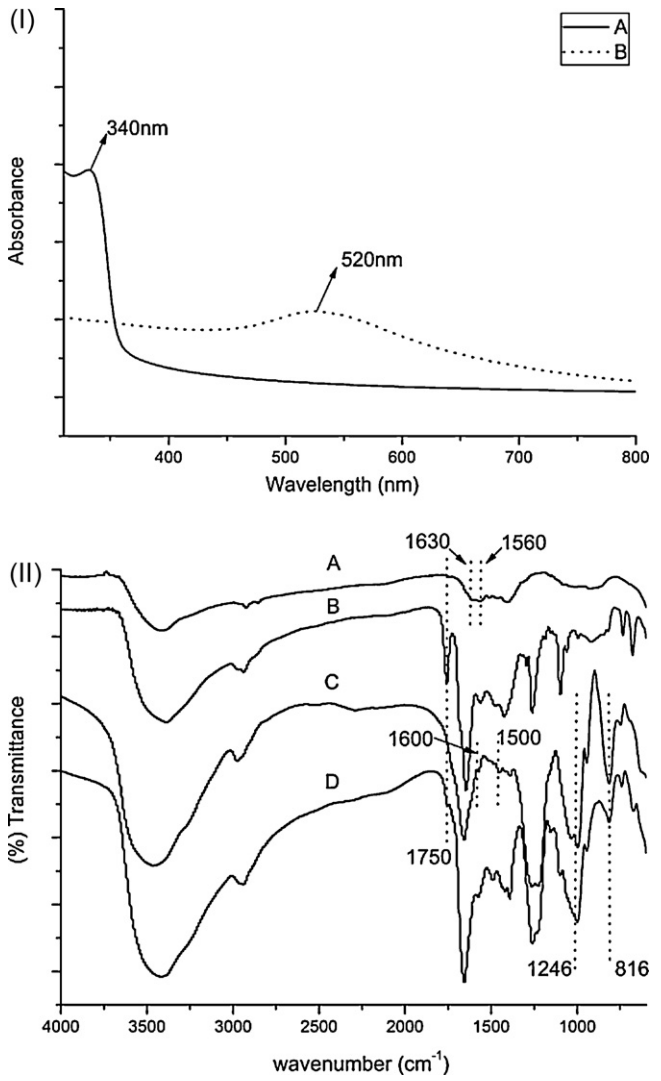

Fig. 2. (I) UV–visible absorption spectra of (A) ZnO QDs; (B) Au NPs. (II) FT-IR spectra of (A) ZnO QDs-conjugated Au NPs; (B) ZnO-Au-PLA-1; (C) GPPS-FA; (D) ZnO-Au-PLA-GPPS-FA-1 NCs.

The primary structures of NCs were identified by comparing their FT-IR absorption bands to those of ZnO QDs-conjugated Au NPs, PLA and GPPS-FA (Fig. 2(II)). The characteristic peaks of the ZnO QDs-conjugated Au NPs appeared at 1630 cm^{-1} and 1560 cm^{-1} (Fig. 2(II)A), assigned to the C═O bond stretching vibration and the —NH vibration of a —$CONH_2$ group. Then a new strong absorption peaks appeared at 1750 cm^{-1} (Fig. 2(II)B), corresponding to the stretching vibrations of C═O groups of PLA on the ZnO-Au-PLA-1, which demonstrated that PLA was modified successfully on the surface of ZnO QDs-conjugated Au NPs. In Fig. 2(II)C, two strong absorption peaks appeared at 1246 cm^{-1} and 816 cm^{-1} for GPPS, assigned to the S═O asymmetric stretching and C—O—S symmetric vibrations, respectively. At the same time, 2-week absorption peaks at 1600 cm^{-1} and 1500 cm^{-1} was due to the characteristic absorption peaks of the benzene ring on the FA. Finally, the FT-IR spectrum of ZnO-Au-PLA-GPPS-FA-1 NCs showed the characteristic absorption bands of both PLA and GPPS-FA (Fig. 2(II)D), confirming successful synthesis of the core–shell structured multifunctional NCs.

Fig. 3 showed the XRD pattern of the ZnO QDs and ZnO-Au-PLA-GPPS-FA-1 NCs. The appearance of diffraction peaks corresponding to (1 0 0), (0 0 2), (1 0 1), (1 0 2), (1 1 0), (1 0 3) and (1 1 2) planes indicated the hexagonal structure of ZnO QDs in all the samples. All

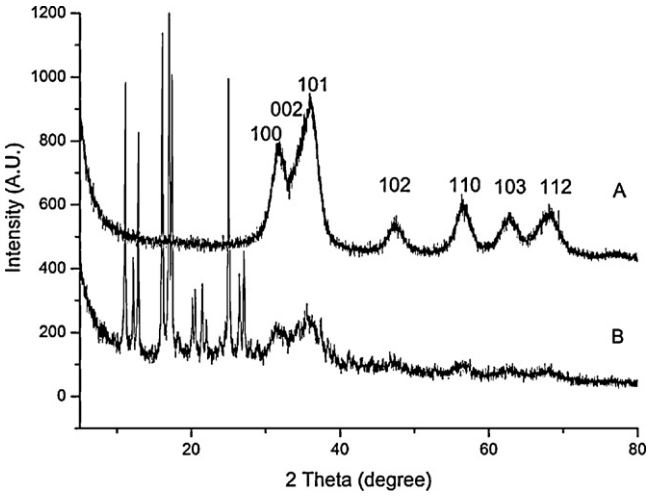

Fig. 3. X-ray diffraction spectra of (A) ZnO QDs; (B) ZnO-Au-PLA-GPPS-FA-1 NCs.

available reflections of the present phases fitted with the Gaussian distribution. The broadening of XRD peaks gave clear indication of formation of nanosized ZnO. Furthermore, all diffraction peaks of ZnO QDs appeared on the ZnO-Au-PLA-GPPS-FA-1 NCs, which indicated that the hexagonal structure of ZnO QDs was not destroyed after ZnO QDs-conjugated polymers. Fig. 3B showed some new diffraction peaks at 2θ regions of 10–30°, which indicated indirectly the good crystallization of polymers (PLA and GPPS-FA) on the surface of ZnO QDs.

Fig. 4A was the photoluminescence (PL) spectra of ZnO QDs, ZnO-Au-PLA-GPPS-FA-1 NCs and ZnO-Au-PLA-GPPS-FA-2 NCs aqueous solutions at the same concentration (1 mg/mL), respectively. The ZnO QDs were excited by 350 nm light to record PL emission, their yellow emission at 570 nm was typical ZnO vacancy luminescence. Furthermore, NCs displayed a symmetric PL emission at 570 nm when excited at 350 nm, which was similar to the PL spectra of ZnO QDs. In our NCs, ZnO QDs-conjugated Au NPs were coated with an inner PLA layer and a subsequent external GPPS-FA layer, but the PL property change of NCs was slight. We speculated that the polymer directly capping on ZnO QDs-conjugated Au NPs core protected the surface electronic structure of ZnO crystals, thus caused a little change of the local optical electric field at the metal surface. The slight variation in the PL intensity was possibly due to the change in the refractive index of the NCs shell when the outer GPPS-FA layer swelled and shrunk (Wu, Zhou, Berliner, Banerjee, & Zhou, 2010). Fig. 4B exhibited strong yellow emission from ZnO QDs, ZnO-Au-PLA-GPPS-FA-1 NCs and ZnO-Au-PLA-GPPS-FA-2 NCs aqueous solutions under UV light (360 nm), and the photograph of aqueous solutions was also presented as a blank comparison.

The size and stability of drug carriers are important properties that influence their performance *in vivo*. These factors will directly affect the biodistribution and circulation time of the carriers. Stable and smaller particle sizes (<200 nm) can reduce the uptake of the reticuloendothelial system (RES) and provide efficient passive tumor-targeting ability *via* the enhanced permeability and retention effects (Schmalenberg, Frauchiger, Nikkhouy-Albers, & Uhrich, 2001). Fig. 5A showed the particle size distribution histogram of ZnO QDs, and ZnO QDs had a narrow size distribution ranging from 3.5 to 5 nm with an average particle size diameter of 4.3 nm. Au NPs also showed a narrow size distribution ranging from 1.5 to 7 nm with an average particle size diameter of 4.6 nm in Fig. 5B. Furthermore, the size distribution of ZnO QDs-conjugated Au NPs was from 8 to 17 nm with an average particle size diameter of 12.2 nm (Fig. 5C), which indicated indirectly that ZnO QDs-conjugated Au NPs was synthesized successfully. In the case of NCs, the size distribution of ZnO-Au-PLA-GPPS-FA-1 NCs and ZnO-Au-PLA-GPPS-FA-2 NCs was relatively broad, ranging from 80 to 150 nm and from 80 to 190 nm, respectively. The average size was 119 nm and 133 nm, respectively (Fig. 5D and E). The increased size and size distribution of NCs might be due to the presence of a fairly thick PLA and GPPS-FA on the surface of Au NPs. These results clearly indicated that the ZnO-Au-PLA-GPPS-FA NCs could form core–shell structured multifunctional drug carriers and stabilize in aqueous solutions.

The size and morphology of ZnO QDs, Au NPs, ZnO-Au-PLA-GPPS-FA-1 NCs and ZnO-Au-PLA-GPPS-FA-2 NCs were further studied by TEM. As shown in Fig. 6A and B, ZnO QDs were spherical with an average diameter of 4 nm, and indicated clearly the highly crystalline nature. Fig. 6C and D showed the lower magnification and high-resolution TEM images of Au NPs. Au NPs showed spherical particles with little agglomeration having sizes 5 nm, and their microcrystal structure could be seen clearly. The size and morphology of ZnO-Au-PLA-GPPS-FA-1 NCs and ZnO-Au-PLA-GPPS-FA-2 NCs was shown in Fig. 6E and F. ZnO-Au-PLA-GPPS-FA-1 NCs and ZnO-Au-PLA-GPPS-FA-2 NCs appeared spherical particles, and the size distribution was in the range of 60–120 nm and 65–155 nm, respectively. The obtained ZnO-Au-PLA-GPPS-FA-2 NCs had a slightly larger average diameter than ZnO-Au-PLA-GPPS-FA-1 NCs due to the diffident M_w of PLA as the inner shell. In addition, NCs was high dispersion due to amphiphilic PLA-GPPS-FA copolymer on the ZnO QDs-conjugated Au NPs core preventing the NCs from aggregation. The diameter of NCs was smaller than their diameter obtained from the DLS experiment. The larger value from the DLS measurement relative to TEM was most likely due to the

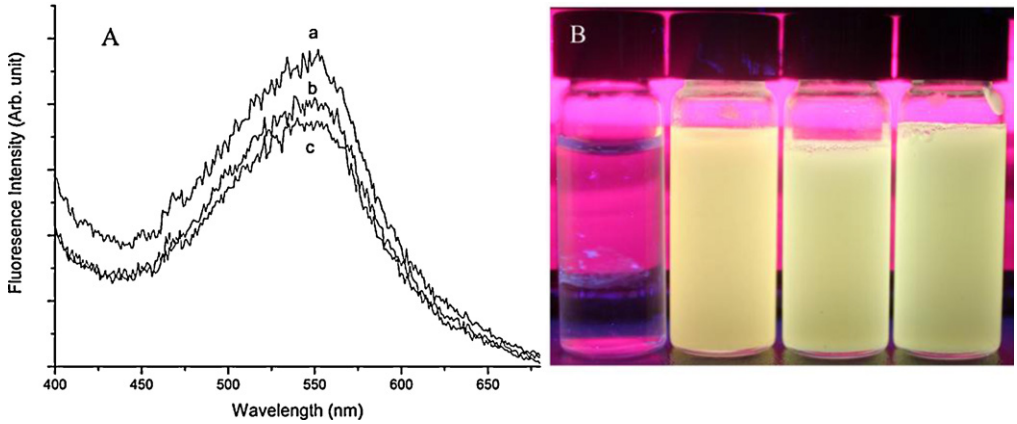

Fig. 4. (A) The typical PL spectra of (a) ZnO QDs; (b) ZnO-Au-PLA-GPPS-FA-1 NCs; (c) ZnO-Au-PLA-GPPS-FA-2 NCs was obtained with the excitation wavelength at 350 nm. (B) The photograph of the samples from left to right was aqueous solutions, ZnO QDs, ZnO-Au-PLA-GPPS-FA-1 NCs and ZnO-Au-PLA-GPPS-FA-2 NCs under UV light (1 mg/mL).

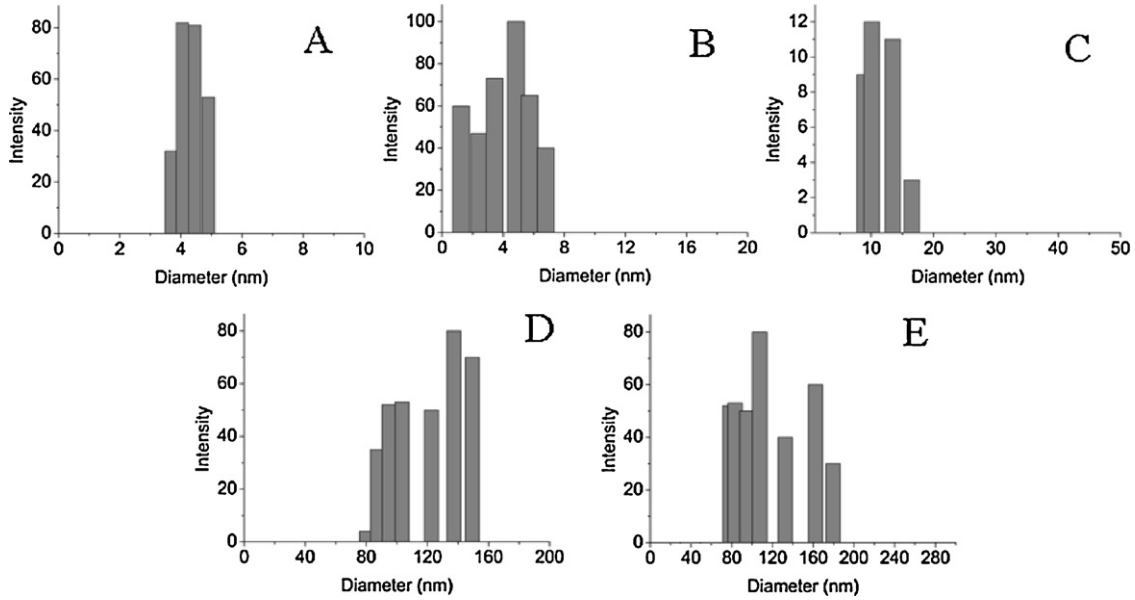

Fig. 5. Size distribution of (A) ZnO QDs; (B) Au NPs; (C) ZnO QDs-conjugated Au NPs; (D) ZnO-Au-PLA-GPPS-FA-1 NCs; (E) ZnO-Au-PLA-GPPS-FA-2 NCs.

existence of a swollen GPPS-FA around the core and the hydration layer around the NCs. The size range of NCs determined by DLS and TEM was desirable for drug carriers to extend their blood circulation time, and the FA-receptor-mediated endocytosis process that leaded to the preferred accumulation of drug-conjugated micelles within tumors (Yuan et al., 1995).

3.3. Drug loading and release

In order to assess the feasibility of NCs as the anticancer drug delivery carrier, we studied drug storage and delivery abilities *in vitro* using ZnO-Au-PLA-GPPS-FA-1 NCs and ZnO-Au-PLA-GPPS-FA-2 NCs under a simulated physiological condition (PBS, pH 7.4) and in an acidic environment (acetate buffer, pH 5.3) at 37 °C. Typically, we loaded the well-dissolved CPT into NCs in DMF solution. An actual drug loading capacity of 6.2 wt% and 8.7 wt% were determined for ZnO-Au-PLA-GPPS-FA-1 NCs and ZnO-Au-PLA-GPPS-FA-2 NCs, respectively. The drug release of free CPT was shown in Fig. 7. A blank release experiment of free CPT solution with an equivalent amount of drug was also performed at pH 7.4. This study suggested that free CPT presented a rapid release (77% of the initial loading amount) in 1 h. Both CPT loaded

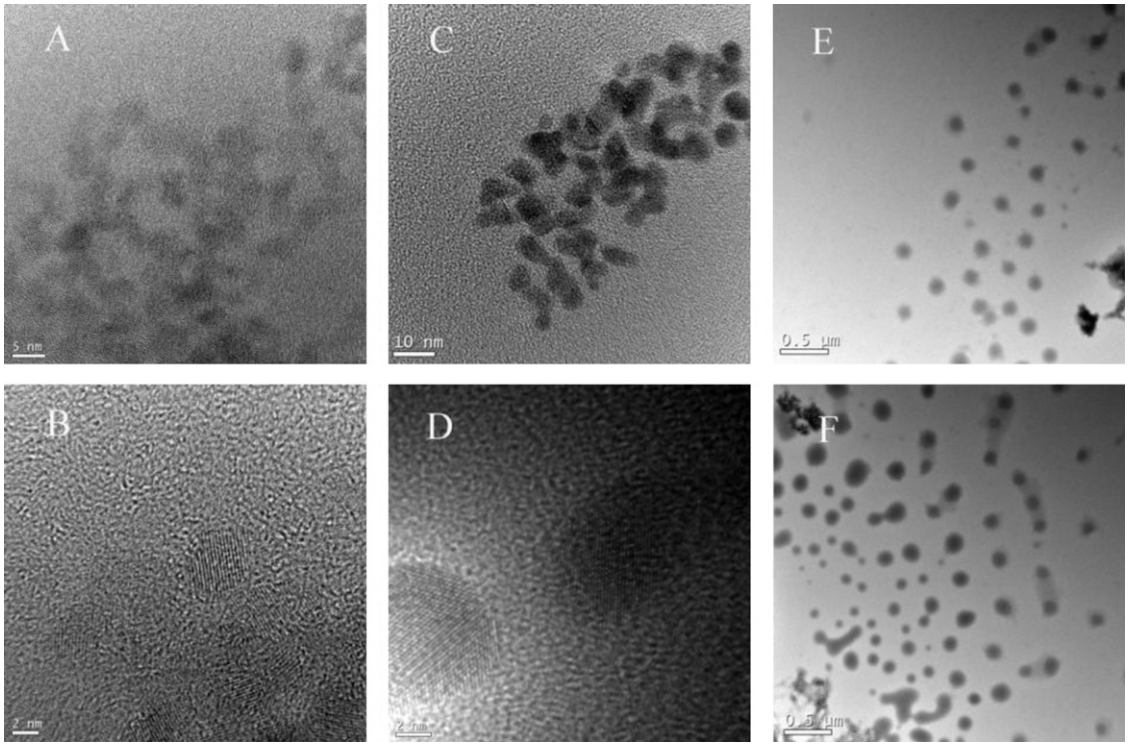

Fig. 6. TEM images of (A) and (B) ZnO QDs; (C) and (D) Au NPs; (E) ZnO-Au-PLA-GPPS-FA-1 NCs; (F) ZnO-Au-PLA-GPPS-FA-2 NCs.

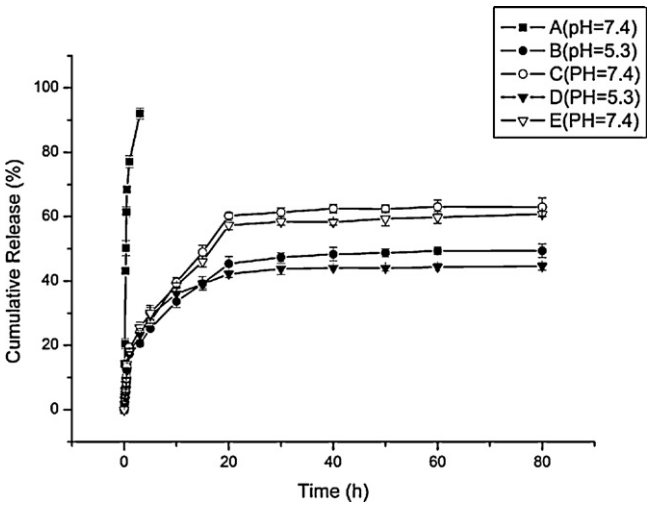

Fig. 7. In the blank release (A), 5 mL free CPT solution was released to 45 mL PBS solution of pH 7.4 at 37 °C. Release profiles of CPT from the CPT-loaded ZnO-Au-PLA-GPPS-FA-1 NCs (B and C) and ZnO-Au-PLA-GPPS-FA-2 NCs (D and E) at neutral (pH 7.4) and acidic conditions (pH 5.3) at 37 °C.

ZnO-Au-PLA-GPPS-FA-1 NCs and CPT loaded ZnO-Au-PLA-GPPS-FA-2 NCs presented a relatively rapid release in the first stage (up to 1 h) followed by a sustained release period (up to 20 h), and then reached a plateau at both pH 7.4 and 5.3. The initial burst release of CPT from the NCs might be attributed to CPT molecules located within the hydrophilic shell. The sustained release of the drug from NCs could be attributed to the hydrophobic–hydrophobic interactions between the drug molecules and the hydrophobic polymer (PLA).

Moreover, the change in pH of the releasing medium could trigger the drug releasing rate in Fig. 7. The amount and rate of CPT release from NCs at pH 7.4 were much greater when compared to that at pH 5.3. At pH 5.3, the initial burst release of CPT for ZnO-Au-PLA-GPPS-FA-1 NCs and ZnO-Au-PLA-GPPS-FA-2 NCs was 16% and 17% of the initial loading amount, respectively. The sustained release of CPT reached a plateau in 20 h, and the release amount was 45% and 42%, respectively. At pH 7.4, the CPT release rate of ZnO-Au-PLA-GPPS-FA-1 NCs and ZnO-Au-PLA-GPPS-FA-2 NCs was faster (19% and 18% of the initial loading amount) in the first 1 h and the sustained release (60% and 58% of the initial loading amount) reached a plateau in 20 h. The increase in pH induced an increase the swelling degree (mesh size) of NCs, which would enhance the mobility of CPT molecules, so that CPT molecules could diffuse out more easily from NCs.

A controlled release behavior of drug from NCs showed that the release obeyed a diffusion-controlled mechanism; however, the diffusion rates at each stage of the drug release differed considerably, suggesting that two different processes might be taking place. In the initial burst stage, drug release occurred faster. During this time, the drug presented on the surface of hydrophilic outer shell might have good access to the surrounding aqueous environment through the NCs surface. However, in the sustained release period, the drug loading could be entrapped in the dense solid regions of

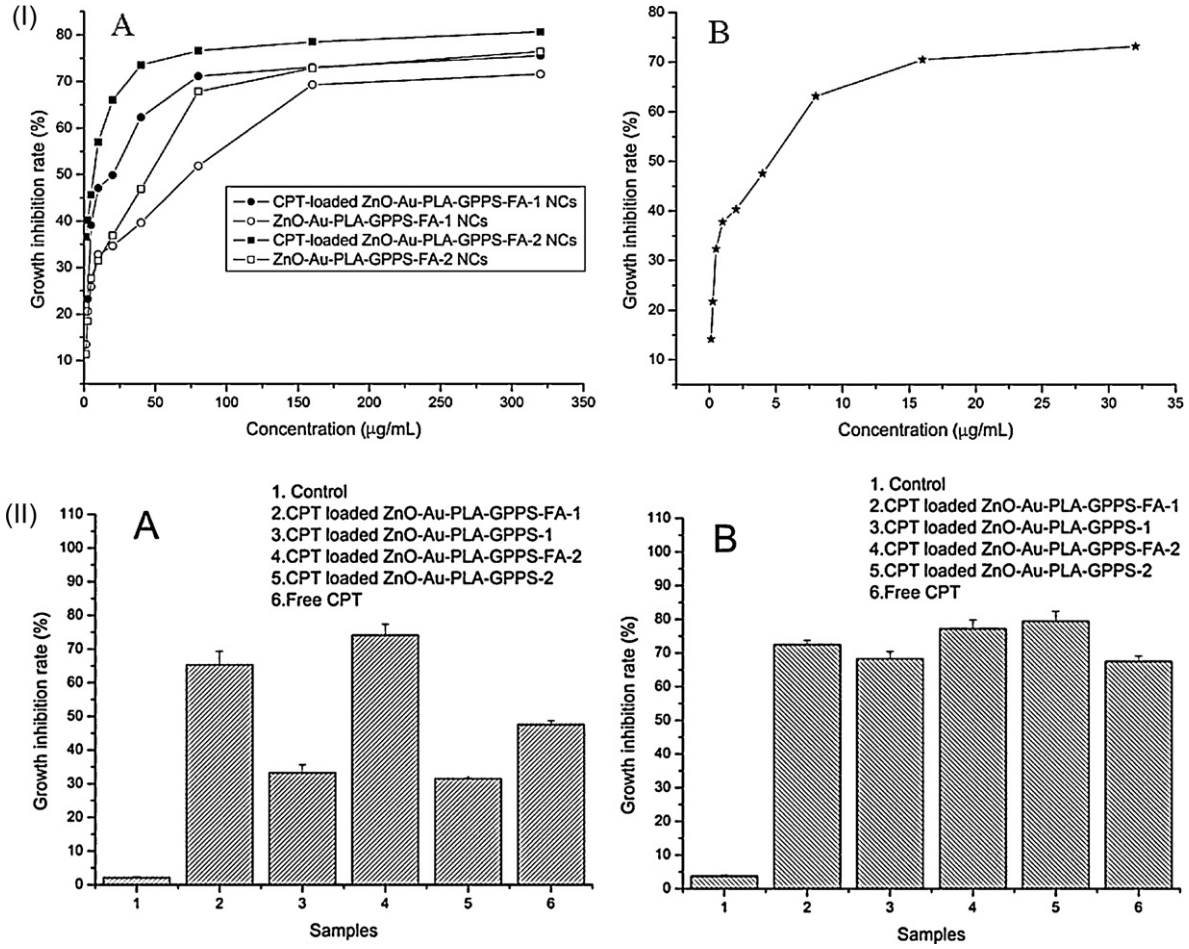

Fig. 8. (I) (A) *In vitro* cytotoxicity of blank ZnO-Au-PLA-GPPS-FA-1 NCs, blank ZnO-Au-PLA-GPPS-FA-2 NCs, the CPT-loaded ZnO-Au-PLA-GPPS-FA-1 NCs and the CPT-loaded ZnO-Au-PLA-GPPS-FA-2 NCs against Hela cells, respectively. (B) The control experiment on the free CPT solution was presented for comparison against Hela cells. (II) Cytotoxicity of free CPT, CPT-loaded ZnO-Au-PLA-GPPS NCs and ZnO-Au-PLA-GPPS-FA NCs against Hela cells (A) and A549 cells (B).

the hydrophobic inner shell where polymer entanglement serves as a much greater impediment to drug transport.

3.4. In vitro cytotoxicity

To evaluate the cytotoxicity of the blank NCs and to verify whether the released CPT was still pharmacologically active, *in vitro* cytotoxicity tests were elaborately conducted against Hela cells that were FA receptor overexpressed cells. The potential cytotoxicity of the free CPT solutions with the corresponding concentrations was also studied. As shown in Fig. 8(I)A, the blank NCs were obvious cytotoxicity to Hela cells at the same concentration of up to 75 μg/mL for ZnO-Au-PLA-GPPS-FA-1 NCs and ZnO-Au-PLA-GPPS-FA-2 NCs. In contrast to this result, the CPT-loaded NCs showed higher cytotoxicity to Hela cells at the same concentration of up to 75 μg/mL for ZnO-Au-PLA-GPPS-FA-1 NCs and ZnO-Au-PLA-GPPS-FA-2 NCs, which included about 4.7 μg/mL and 6.5 μg/mL free CPT in both systems, respectively. Furthermore, the inhibition rates of the CPT-loaded NCs in Fig. 8(I)A were higher than that of the free CPT in Fig. 8(I)B since the CPT amounts were at the same levels.

These results indicated that both the blank NCs and the CPT-loaded NCs provided high anticancer activity. The cytotoxicity of CPT-loaded NCs was slightly higher than that of free CPT at all the studied concentrations. This was likely because the NCs had certain antitumor activities due to GPPS on the surface of the NCs, but had no obvious cytotoxicity to noncancerous cells, which would be more effective to kill tumor cells by the cooperation of carriers and drugs. Thus, the slightly higher cytotoxicity of the CPT-loaded NCs than the free CPT solutions was understandable.

3.5. In vitro FA targeting

To directly define a role for FA targeting, free CPT (4 μg/mL), and CPT loaded nanocarriers (CPT concentration: 4 μg/mL) were studied against Hela cells (folate receptor over-expressing cell line) and A549 cells (folate receptor deficient cell line). As shown in Fig. 8(II)A, compared with CPT loaded ZnO-Au-PLA-GPPS-1 NCs and ZnO-Au-PLA-GPPS-2 NCs, CPT loaded ZnO-Au-PLA-GPPS-FA-1 NCs and ZnO-Au-PLA-GPPS-FA-2 NCs exhibited higher inhibition ratio against Hela cells. The results showed that FA molecules in CPT loaded nanocarriers played an important role in enhancing cytotoxic effect by binding of CPT loaded nanocarriers with FA receptors on Hela cells, and increasing their intracellular uptake as a result of the receptor-mediated endocytosis. However, there was no significant difference in inhibition ratio of A549 cells when cultured in the presence of ZnO-Au-PLA-GPPS NCs and ZnO-Au-PLA-GPPS-FA NCs (Fig. 8(II)B). This observation showed that the FA molecule present on the surface of nanocarriers did not have any effect on the A549 cells cellular uptake. The observed cytotoxicity may be due to the cellular uptake of CPT in the nanocarriers which could diffuse into the cells.

4. Conclusion

FA-conjugated amphiphilic ZnO-Au-PLA-GPPS-FA NCs were synthesized as the tumor-targeted drug delivery carriers. NCs displayed strong yellow emission at 570 nm. The release *in vitro* indicated that the NCs could be a very promising vehicle for the administration of controlled release of hydrophobic anticancer drugs. The strong hydrophobic interactions of the hydrophobic PLA with the drug molecules could be a main reason for the slow and steady release of the CPT from the NCs. The CPT release from NCs at pH 7.4 was much greater than that at pH 5.3. The cytotoxicity studies showed that both the blank NCs and the CPT-loaded NCs provided high anticancer activity. This could be because the NCs had certain antitumor activities due to GPPS on the surface of the NCs, which would be more effective to kill tumor cells by the cooperation of carriers and drugs. Furthermore, CPT-loaded nanocarriers gained specificity to target some cancer cells due to the enhanced cell uptake mediated by FA moiety. These results indicated that the ZnO-Au-PLA-GPPS-FA NCs could not only be an excellent tumor-targeted drug delivery nanocarrier, but also had an assistant role in the treatment of cancer.

Acknowledgements

This work was supported by the Fundamental Research Funds for the Central Universities (no. lzujbky-2012-k09) and the National Natural Science Foundation of China (NSFC) Fund (no. 21105039).

Appendix A. Supplementary data

Supplementary data associated with this article can be found, in the online version, at http://dx.doi.org/10.1016/j.carbpol.2012.10.022.

References

Alivisatos, A. P., Gu, W. W., & Larabell, C. (2005). Quantum dots as cellular probes. *Annual Review of Biomedical Engineering*, *7*, 55–76.
Bahadur, K. C. R., Aryal, S., Bhattarai, N., & Kim, H. Y. (2006). Ceramic modification of N-acylated chitosan stabilized gold nanoparticles. *Scripta Materialia*, *54*, 2029–2034.
Birgitte, L. C., Per, M., & Zhao, Y. (1995). Traditional Chinese medicine in treatment of hyperlipidaemia. *Journal of Ethnopharmacology*, *46*, 125–129.
Bottrill, M., & Mark, G. (2011). Some aspects of quantum dot toxicity. *Chemical Communications*, *47*, 7039–7050.
Chan, W. C. W., & Nie, S. (1998). Quantum dot bioconjugates for ultrasensitive nonisotopic detection. *Science*, *281*, 2016–2018.
Chen, T., Li, B., Li, Y. Y., Zhao, C. D., Shen, J. M., & Zhang, H. X. (2011). Catalytic synthesis and antitumor activities of sulfated polysaccharide from *Gynostemma pentaphyllum* Makino. *Carbohydrate Polymers*, *83*, 554–560.
Cheng, Y., Samia, A. C., Li, J., Kenney, M. E., Resnick, A., & Burda, C. (2010). Delivery and efficacy of a cancer drug as a function of the bond to the gold nanoparticle surface. *Langmuir*, *26*, 2248–2255.
Duncan, B., Kim, C., & Vincent, M. (2010). Gold nanoparticle platforms as drug and biomacromolecule delivery systems. *Journal of Controlled Release*, *148*, 122–127.
Ghosh, P., Han, G., De, M., Kim, C. K., & Rotello, V. M. (2008). Gold nanoparticles in delivery applications. *Advanced Drug Delivery Reviews*, *60*, 1307–1321.
Gu, F. X., Karnik, R., Wang, A. Z., Alexis, F., Levy-Nissenbarum, E., & Hong, S. (2007). Targeted nanoparticles for cancer therapy. *Nano Today*, *2*, 14–21.
Jain, K. K. (2005). Targeted drug delivery for cancer. *Technology in Cancer Research & Treatment*, *4*, 311–316.
Jain, P. K., Ih, E. S., & Ma, E. S. (2007). Au nanoparticles target cancer. *Nano Today*, *2*, 18–29.
Jana, R., Gearheart, L., & Murphy, J. (2001). Wet chemical synthesis of high aspect ratio cylindrical gold nanorods. *The Journal of Physical Chemistry B*, *105*, 4065.
Leamon, C. P., & Low, P. S. (1991). Delivery of macromolecules into living cells – a method that exploits folate receptor endocytosis. *Proceedings of the National Academy of Sciences of the United States of America*, *88*, 5572–5577.
Luo, S., Xu, J., Zhang, Y., Liu, S., & Wu, C. (2005). Double hydrophilic block copolymer monolayer protected hybrid gold nanoparticles and their shell cross-linking. *The Journal of Physical Chemistry B*, *109*, 22159–22166.
Male, K. B., Lachance, B., Hrapovic, S., Sunahara, G., & Luong, J. H. T. (2008). Assessment of cytotoxicity of quantum dots and gold nanoparticles using cell-based impedance spectroscopy. *Analytical Chemistry*, *80*, 5487–5493.
Medintz, I. L., Uyeda, H. T., Goldman, E. R., & Mattoussi, H. (2005). Quantum dot bioconjugates for imaging, labelling and sensing. *Nature Materials*, *4*, 435–446.
Meulenkamp, E. A. (1998). Synthesis and growth of ZnO nanoparticles. *The Journal of Physical Chemistry B*, *102*, 5566–5572.
Michalet, X., Pinaud, F. F., Bentolila, L. A., Tsay, J. M., Doose, S., & Li, J. J. (2005). Quantum dots for live cells, *in vivo* imaging, and diagnostics. *Science*, *307*, 538–544.
Moussodia, R. O., Balan, L., Merlin, C., Mustin, C., & Schneider, R. (2010). Biocompatible and stable ZnO quantum dots generated by functionalization with siloxane-core PAMAM dendrons. *Journal of Materials Chemistry*, *20*, 1147–1155.
Patra, M. K., Manoth, M., Singh, V. K., Siddaramana Gowd, G., Choudhry, V. S., Vadera, S. R., et al. (2009). Synthesis of stable dispersion of ZnO quantum dots in aqueous medium showing visible emission from bluish green to yellow. *Journal of Luminescence*, *129*, 320–324.
Prabaharan, M., Grailer, J. J., Pilla, S., Steeber, D. A., & Gong, S. Q. (2009a). Gold nanoparticles with a monolayer of doxorubicin-conjugated amphiphilic block copolymer for tumor-targeted drug delivery. *Biomaterials*, *30*, 6065–6075.
Prabaharan, M., Grailer, J. J., Pilla, S., Steeber, D. A., & Gong, S. Q. (2009b). Folate-conjugated amphiphilic hyperbranched block copolymers based on Boltorn H40,

poly(L-lactide) and poly(ethylene glycol) for tumor-targeted drug delivery. *Biomaterials*, *30*, 3009–3019.
Qian, X. H., Wang, Y. X., & Tang, X. L. (1998). Effects of *Gynostemma pentaphllum* Makino polysaccharide (PGP) on immunefunction. *Journal of China Pharmaceutical University*, *30*, 51–53.
Reum, N., Fink-Straube, C., Klein, T., Hartmann, R. W., Lehr, C. M., & Schneider, M. (2010). Multilayer coating of gold nanoparticles with drug–polymer coadsorbates. *Langmuir*, *26*, 16901–16908.
Rujjanawate, C., Kanjanapothi, D., & Amornlerdpison, D. (2004). The antigastric ulcer effect of *Gynostemma pentaphyllum* Makino. *Phytomedicine*, *11*, 431–435.
Sarah, D., Brown Nativo, P., Smith, J. A., Stirling, D., & Edwards, P. R. (2010). Gold nanoparticles for the improved anticancer drug delivery of the active component of oxaliplatin. *Journal of the American Chemical Society*, *132*, 4678–4684.
Schmalenberg, K. E., Frauchiger, L., Nikkhouy-Albers, L., & Uhrich, K. E. (2001). Cytotoxicity of a unimolecular polymeric micelle and its degradation products. *Biomacromolecules*, *2*, 851–856.
Turek, J. J., Leamon, C. P., & Low, P. S. (1993). Endocytosis of folate-protein conjugates – ultrastructural-localization in Kb cells. *Journal of Cell Science*, *106*, 423–430.
Viswanatha, R., Chakraborty, S., Basu, S., & Sarma, D. D. (2006). Blue-emitting copper-doped zinc oxide nanocrystals. *The Journal of Physical Chemistry B*, *110*, 22310–22311.
Wu, W., Zhou, T., Berliner, A., Banerjee, P., & Zhou, S. (2010). Smart core–shell hybrid nanogels with Ag nanoparticle core for cancer cell imaging and gel shell for pH-regulated drug delivery. *Chemistry of Materials*, *22*, 1966–1976.
Wu, W. T., Shen, J., Banerjee, P., & Zhou, S. Q. (2010). Core–shell hybrid nanogels for integration of optical temperature-sensing, targeted tumor cell imaging, and combined chemo-photothermal treatment. *Biomaterials*, *31*, 7555–7566.
Wyrna, D., & Beyer, N. (2002). One-dimensional arrangements of metal nanoclusters. *Nano Letter*, *2*, 419–421.
Xiong, H. M., Xu, Y., Ren, Q. G., & Xia, Y. Y. (2008). Stable aqueous ZnO@polymer core–shell nanoparticles with tunable photoluminescence and their application in cell imaging. *Journal of the American Chemical Society*, *130*, 7522–7523.
Yuan, F., Dellian, M., Fukumura, D., Leunig, M., Berk, D. A., & Torchilin, V. P. (1995). Vascular permeability in a human tumor xenograft: Molecular size dependence and cutoff size. *Cancer Research*, *55*, 3752–3757.
Yuan, L., Tang, Q. Q., Yang, D., Zhang, J. Z., Zhang, F. Y., & Hu, J. H. (2011). Preparation of pH-responsive mesoporous silica nanoparticles and their application in controlled drug delivery. *The Journal of Physical Chemistry C*, *115*, 9926–9932.
Yuan, Q., Hein, S., & Misra, R. D. K. (2010). New generation of chitosan encapsulated ZnO quantum dots with drug: Synthesis, characterization, and in-vitro drug delivery response. *Acta Biomaterialia*, *6*, 2732–2739.
Zeng, H., Li, Z., Cai, W., Cao, B., Liu, P., & Yang, S. (2007). Microstructure control of Zn/ZnO core/shell nanoparticles and their temperature-dependent blue emissions. *The Journal of Physical Chemistry B*, *111*, 14311–14317.
Zhu, Y. F., Fang, Y., & Kaskel, S. (2010). Folate-conjugated Fe_3O_4@SiO_2 hollow mesoporous spheres for targeted anticancer drug delivery. *The Journal of Physical Chemistry C*, *114*, 16382–16388.